A Drug-Loaded Aptamer–Gold Nanoparticle Bioconjugate for Combined CT Imaging and Therapy of Prostate Cancer

Dongkyu Kim,[†] Yong Yeon Jeong,[‡] and Sangyong Jon[†,*]

[†]Cell Dynamics Research Center, Research Center for Biomolecular Nanotechnology, School of Life Sciences, Gwangju Institute of Science and Technology, 261 Chemdan-gwagiro, Gwangju 500-712, Republic of Korea, and [‡]Department of Diagnostic Radiology, Chonnam National University Hwasun Hospital, 160 Ilsim-ri, Hwasun-eup, Jeonnam 519-809, Republic of Korea

ABSTRACT Computed tomography (CT) is one of the most useful diagnostic tools among commonly used biomedical imaging techniques, which also include magnetic resonance imaging (MRI), positron emission tomography (PET), and ultrasound. However, currently available CT contrast agents, which are based on small iodinated molecules, possess a number of limitations, including a lack of targeted molecular imaging, short imaging time, and renal toxicity. Here, we report a multifunctional nanoparticle for targeted molecular CT imaging and therapy of prostate cancer. By functionalizing the surface of gold nanoparticles (GNPs) with a prostate-specific membrane antigen (PSMA) RNA aptamer that binds to PSMA, we established a targeted molecular CT imaging system capable of specific imaging of prostate cancer cells that express the PSMA protein. The resulting PSMA aptamer-conjugated GNP showed more than 4-fold greater CT intensity for a targeted LNCaP cell than that of a nontargeted PC3 cell. Furthermore, the PSMA aptamer-conjugated GNPs after loading of doxorubicin were significantly more potent against targeted LNCaP cells than against nontargeted PC3 cells.

KEYWORDS: computed tomography (CT) · aptamer · gold nanoparticle · targeted molecular imaging · drug delivery

Advances in nanotechnology have enabled the development of multifunctional nanoparticles that can simultaneously perform various functions, including targeting, imaging, and therapy.[1–9] Recently, superparamagnetic iron oxide nanoparticles,[10–12] quantum dots,[13–15] and gold nanoparticles[16,17] have been investigated for potential multifunctional uses as therapeutic agents, delivery vehicles and imaging agents capable of visualization by magnetic resonance imaging (MRI) or optical imaging techniques. Of the various medical imaging systems available, computed tomography (CT) is one of the most frequently used hospital diagnostic tools and also one of the most cost-effective. Recently, we reported the synthesis of polyethylene glycol (PEG)-coated gold nanoparticles (GNPs) for use as a novel CT contrast agent in blood pool imaging (angiography) and for diagnosis of hepatoma *in vivo* and suggested that GNP-based CT contrast agents might be capable of overcoming the limitations of conventional iodine-based contrast agents.[18] Very recently, Popvtzer and colleagues reported that antibody-conjugated GNPs selectively bound to target cancer cells and showed that such GNP–cancer cell interaction could be imaged by CT instruments.[19] However, GNP-based multifunctional nanoparticles with the tripartite capacity to mediate targeting, CT imaging, and drug delivery to target cancer cells have not yet been developed.

Aptamers are an emerging class of targeting ligands that also serve as biological drugs that can be used to treat various diseases.[20–26] As escort molecules, aptamers are able to deliver drugs,[6,13,26] or nanoparticles encapsulating drugs,[21–23] to target cells *via* high-affinity, specific binding. Recently, we showed that a prostate-specific membrane antigen (PSMA)-specific aptamer formed a 1:1 physical complex with doxorubicin (Dox) *via* intercalation, and thereby delivered this anticancer drug to target prostate cancer cells.[26] Thus, the PSMA aptamer (A10 RNA aptamer) described in our previous study served the dual functions of escort molecule and drug delivery carrier.

Here we report that PSMA-specific, aptamer-conjugated multifunctional GNPs are able to act as anticancer drug delivery vehicles and as CT nanocontrast agents because of the presence of gold, resulting in combined prostate cancer imaging and anticancer therapy.

*Address correspondence to syjon@gist.ac.kr.

Received for review December 22, 2009 and accepted June 08, 2010.

Published online June 15, 2010.
10.1021/nn901877h

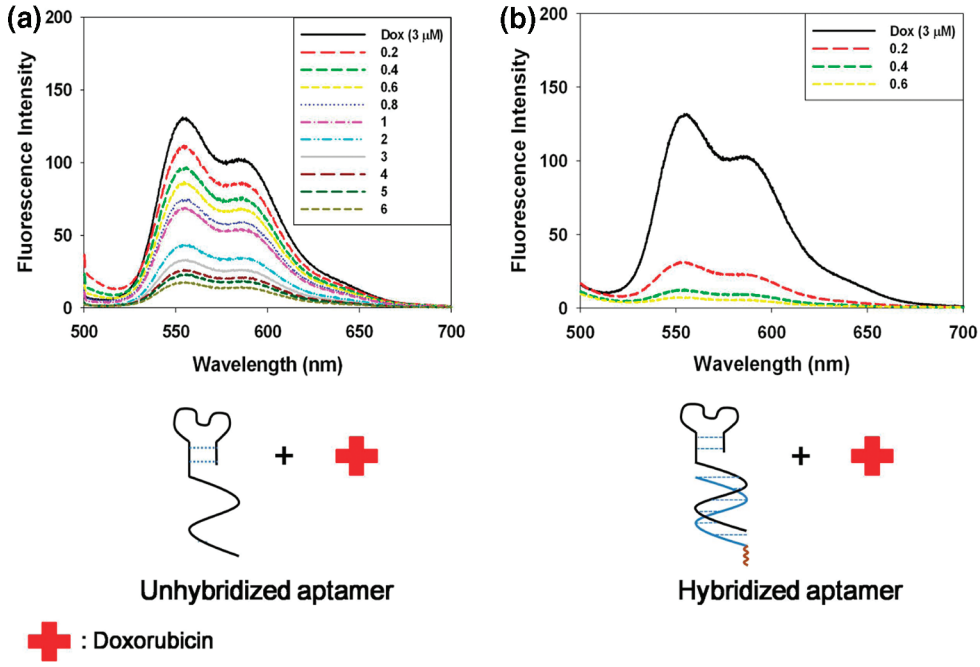

Figure 1. Fluorescence spectra of a Dox solution (3 μM) with increasing molar ratios of (a) unhybridized aptamer (from top to bottom: 0, 0.2, 0.4, 0.6, 0.8, 1, 2, 3, 4, 5, and 6 equiv) and (b) hybridized aptamer (from top to bottom: 0, 0.2, 0.4, and 0.6 equiv).

RESULTS AND DISCUSSION

In the present study, we used a PSMA-specific A9 RNA aptamer with a 21-base $(CGA)_7$ extension at the 3′ end. Because Dox intercalates preferentially into consecutive −CG− base pairs,[27] fusing of the $(CGA)_7$ repeating oligonucleotide (ONT) to the original PSMA aptamer significantly enhanced Dox-loading capacity, providing binding sites for at least 6−7 Dox molecules in the extended region instead of the single Dox molecule bound by the original PSMA aptamer.

To determine how many Dox molecules could actually be loaded onto the PSMA aptamer−$(CGA)_7$ after hybridization with the complementary sequence, 5′-$(TCG)_7$-3′, we measured Dox intercalation by monitoring Dox fluorescence quenching. As the amount of added unhybridized or hybridized aptamer increased, there was a sequential decrease in the native fluorescence spectrum of Dox that ultimately reached a maximum level of fluorescence quenching (Figure 1). Consistent with predictions, the loading capacity of the hybridized aptamer was 7.5 Dox per aptamer and was much higher than that of the unhybridized aptamer (0.6 Dox per aptamer). On the basis of this result, we introduced the PSMA aptamer with the $(CGA)_7$ extension onto the surface of GNPs, with the goal of achieving high-level drug loading. A schematic depiction of the preparation of Dox-loaded aptamer−GNP conjugates is shown in Figure 2. Citrate-stabilized GNPs, serving the CT contrast agent function, were synthesized using a citrate reduction method.[28] In the first step, citrate-stabilized GNPs were coated with 5′-SH-functionalized capture ONTs composed of an A_{10} spacer and a $(TCG)_7$ ONT, which hybridizes with the PSMA aptamer−$(CGA)_7$ and creates the double-stranded GC-rich region that accommodates multiple Dox molecules. In the second step, the PSMA aptamer−$(CGA)_7$, serving both targeting and drug carrier functions, was conjugated to the capture ONT-modified GNPs *via* hybridization between the capture sequence and the extended sequence of the PSMA aptamer. Dynamic light scattering was used to measure the hydrodynamic size of the GNPs and to confirm that capture ONTs and the extended aptamers were conjugated sequentially in the manner illustrated in Figure 2. The diameter of citrate-stabilized GNPs was 12.7 ± 3.3 nm. After immobilization of capture ONTs, NP diameter increased to 21.3 ± 5.8 nm and was further increased to 29.4 ± 7.7 nm by subsequent hybridization of PSMA aptamer−$(CGA)_7$, suggesting that capture ONTs and aptamers were sequentially introduced onto the surface of GNPs. The extent magnitude of the observed size increase was in good agreement with the data of Javier and colleagues (Figure 3).[29] In the final step, Dox was loaded onto PSMA aptamer-conjugated GNPs *via* intercalation. The amount of Dox loaded was 615 ± 34 Dox molecules per GNP, calculated indirectly by measuring the amount of unloaded Dox remaining after purification of the drug-loaded conjugate by centrifugation. On the basis of the estimate of 7.5 loadable Dox molecules per hybridized PSMA aptamer−$(CGA)_7$/$(TCG)_7$ ONT, it may be inferred that each GNP contained approximately 82 copies of the hybridized aptamer.

We next examined whether PSMA aptamer-conjugated GNPs could preferentially bind to target LNCaP prostate epithelial cells that overexpressed PSMA antigen in the plasma membrane. PC3 prostate epithe-

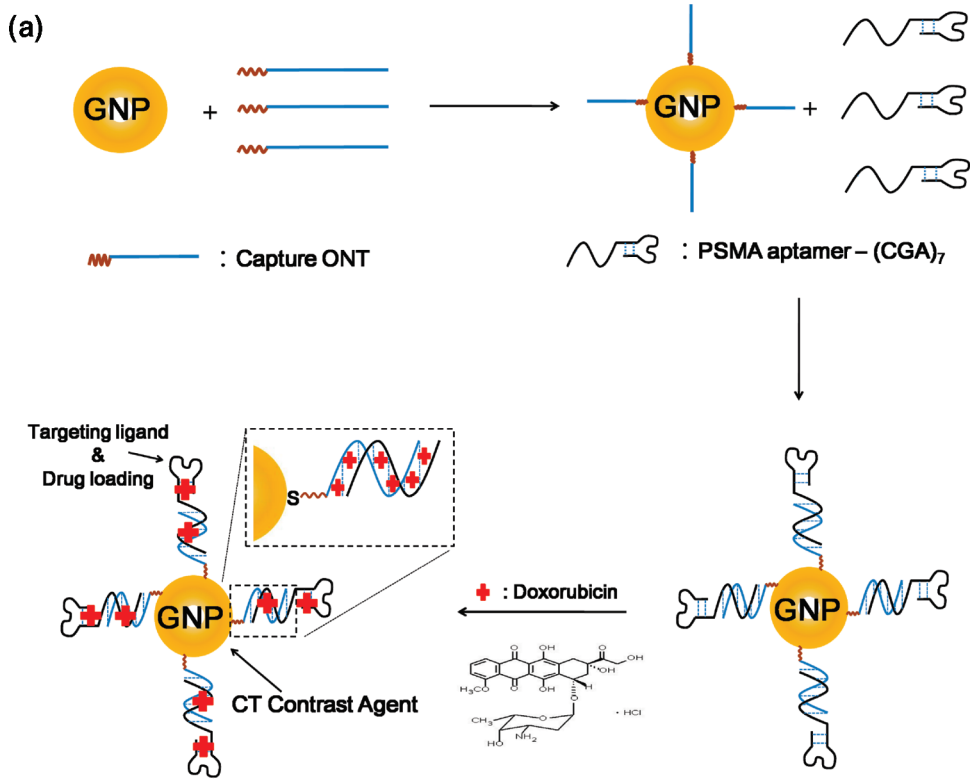

(b)

PSMA aptamer – $(CGA)_7$: 5′ - GGGAGGACGAUGCGGACCGAAAAAGACCUGACUUCUAUACUAAGUCUA CGUUCCCAGACGACUCGCCCGACGACGACGACGACGACGACGA – 3′
(under line : extended sequence)

Capture ONT : 5′ - SH – $(A)_{10}$ – TCGTCGTCGTCGTCGTCGTCG – 3′

Figure 2. (a) Schematic illustration of the method for preparing Dox-loaded aptamer-conjugated GNPs. (b) PSMA aptamer and ONT sequences used to synthesize Dox-loaded aptamer-conjugated GNPs.

lial cells, which do not express detectable levels of PSMA, were used as a negative control. Cells were incubated with PSMA aptamer-conjugated GNPs (1 nM) or OPTI-MEM medium only (control) at 37 °C for 2 h and next washed with phosphate buffered saline (PBS) to remove unbound NPs. The molar concentration of GNPs was measured by UV−vis spectrophotometry (molar extinction coefficient for 13 nm GNP at 520 nm: 2.7×10^8 M^{-1} cm^{-1}).[30] To visualize GNPs, we stained treated cells using a silver enhancement kit. Figure 4 shows silver-stained optical images of LNCaP and PC3 cells incubated with or without PSMA aptamer-conjugated GNPs. There were no clear black spots in the magnified images of either cell type after incubating in medium alone (Figure 4a,c). However, as seen in the magnified image of Figure 4b, numerous black spots representing aggregated silver metal deposited on GNPs were clearly identifiable in LNCaP cells after treatment with extended PSMA aptamer-conjugated GNPs. In contrast, no such silver-enhanced spots were detectable in PC3 cells treated with the same GNP conjugate. Furthermore, inductively coupled plasma atomic emission spectroscopy (ICP-AES) was used to quantify the PSMA aptamer-conjugated GNPs that were taken up by cells. ICP-AES analysis revealed that uptake of the PSMA aptamer-conjugated GNPs by LNCaP cells was ~3 times higher than that by PC3 (Figure S1 in the Supporting Information). These results clearly indicate that hybridized PSMA aptamer-conjugated GNPs have the ability to bind specifically to target LNCaP prostate cancer cells.

Next, we investigated the ability of hybridized aptamer-conjugated GNPs to serve as a targeted CT contrast agent. LNCaP and PC3 cells were incubated with hybridized aptamer-conjugated GNPs (5 nM) at 37 °C for 6 h, washed three times with PBS, and resuspended in 100 μL of PBS. The attenuation of CT intensity is expressed in Hounsfield units (HU) and was measured using clinical CT at 80 kVp after immersing each sample in a water bath (Figure 5). Figure 5a shows the actual CT images of LNCaP and PC3 cells incubated with or without PSMA aptamer-conjugated GNPs. The CT image of LNCaP cells treated with PSMA aptamer-conjugated GNPs was much brighter than that of PC3 cells treated with the same GNPs, and these latter images were similar to CT images of nontreated LNCaP and PC3 cells, the scramble aptamer-conjugated GNPs treated LNCaP cells, and PBS-only controls. A quantitative analysis of the CT intensity of each sample is shown

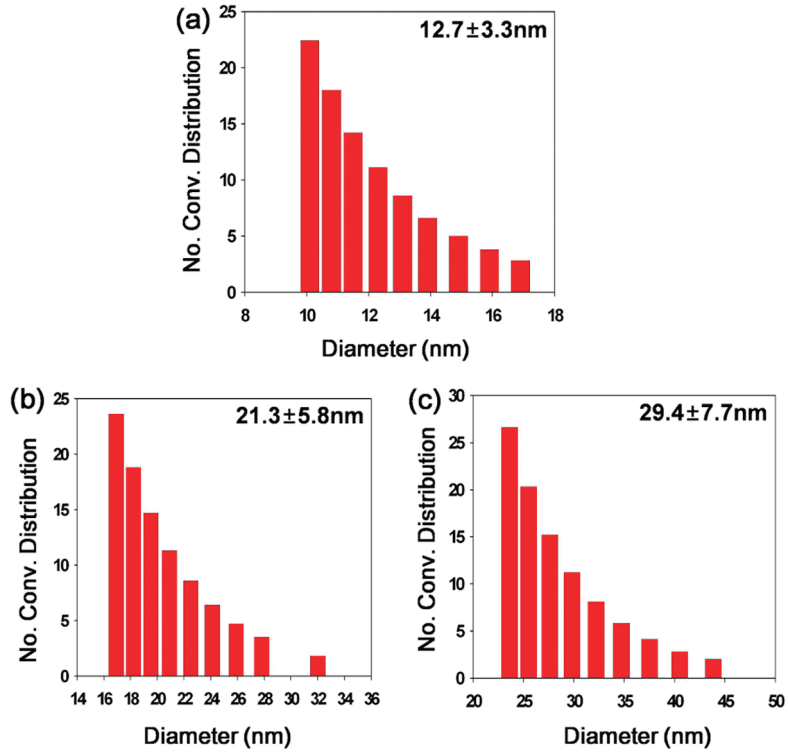

Figure 3. Hydrodynamic size distribution of (a) citrate-stabilized GNPs, (b) 5′-HS-A_{10}-$(TCG)_7$-3′-modified GNPs, and (c) GNPs conjugated with PSMA aptamer−$(CGA)_7$ *via* hybridization.

in Figure 5b. The HU value for LNCaP cells treated with PSMA aptamer-conjugated GNPs (130 ± 17 HU) was more than 4-fold greater than that for PC3 cells (28 ± 3 HU). In contrast, little difference in the HU values is observed between nontreated and the scramble aptamer-conjugated GNP-treated LNCaP cells, indicating high target specificity of the PSMA aptamer. These results suggest that PSMA aptamer-conjugated GNPs have the potential to be used as a CT contrast agent to detect prostate cancer with high sensitivity and specificity.

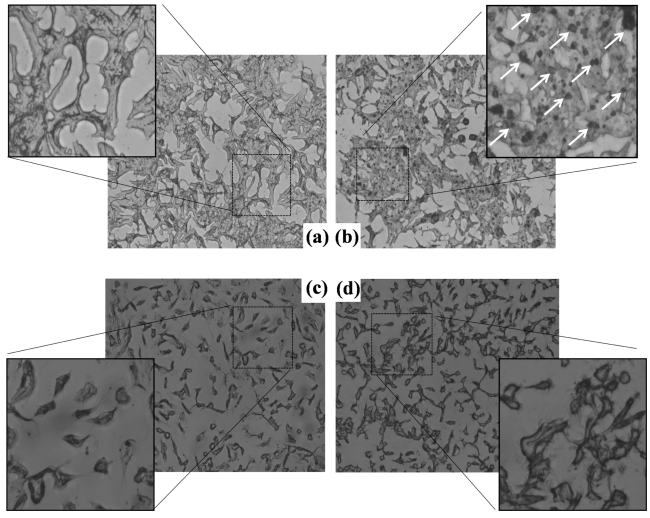

Figure 4. Silver-stained optical microscope images of LNCaP cells (a,b) and PC3 cells (c,d) following different 2 h treatments. (a) LNCaP and (c) PC3 cells incubated with OPTI-MEM medium (negative control). (b) LNCaP and (d) PC3 cell treated with 1 nM PSMA aptamer-conjugated GNPs. White arrows indicate silver-enhanced GNPs.

After demonstrating the potential of hybridized aptamer-conjugated GNPs as a targeted CT contrast agent, we next examined the potential use of the GNPs as a drug delivery carrier. Dox-loaded PSMA aptamer-conjugated GNPs, prepared as illustrated in Figure 2, contained approximately 615 Dox molecules per GNP. Because Dox is a fluorescent molecule and has an ability to penetrate plasma cellular membrane, it is easy to examine whether or not the drug is delivered to target cells. After treating LNCap and PC3 cells with Dox-loaded aptamer-conjugated GNPs, uptake of Dox by each cell was assessed by confocal laser scanning microscopy (CLSM) and flow cytometry. In the CLSM images, strong fluorescence was observed mostly in the cytoplasm of LNCaP cells, whereas no fluorescence signal was seen in PC3 cells (Figure S2 in the Supporting Information), indicating that highly selective, differential delivery of Dox to target cancer cells was attained. Furthermore, distinct shift of cell population with high fluorescence was observed for the conjugate GNP-treated LNCaP cells but not for the case of PC3 cells in the flow cytometry experiment (Figure S3 in the Supporting Information). These results clearly demonstrate the feasibility of aptamer-conjugated GNPs as a drug delivery vehicle in a targeted manner. Although GNPs are generally known to be biocompatible and nontoxic, we evaluated the toxicity of PSMA aptamer-conjugated GNPs by measuring cell viability using MTT (3-4,5-dimethylthiazol-2-yl-2,5-diphenyl tetrazolium bromide) assays. As shown in Figure 6a, LNCaP and PC3 cells incubated for 24 h with increasing amounts of PSMA

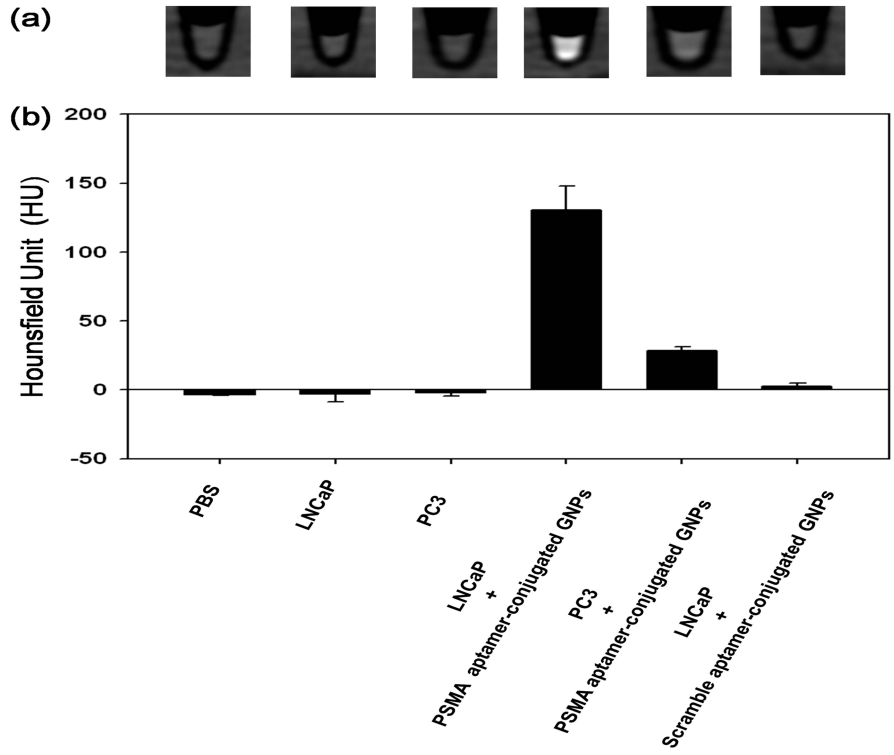

Figure 5. (a) CT images and (b) HU values of PBS, LNCaP, PC3 cells, and LNCaP and PC3 cells treated with PSMA aptamer-conjugated GNPs (5 nM) or scramble aptamer-conjugated GNPs (5 nM) for 6 h ($n = 3$).

aptamer-conjugated GNPs exhibited no appreciable loss of viability, even at conjugate concentrations as high as 20 nM, a concentration much higher than that needed to load 5 μM Dox. Next, we examined the cytotoxic effect of parent Dox (5 μM) and Dox-loaded aptamer-conjugated GNPs (5 μM Dox equivalent) on LNCaP and PC3 cells (Figure 6b). MTT assays revealed that Dox-loaded aptamer-conjugated GNPs were significantly more cytotoxic toward targeted LNCaP cells than the nontargeted PC3 cells (cell viability 50 ± 6% for LNCaP *versus* 71 ± 6% for PC3; $p < 0.05$, $n = 5$). The difference in the cytotoxicity result is considered more significant because parent Dox killed PC3 cells slightly more effectively than LNCaP cells (cell viability 60 ± 8% for LNCaP *versus* 51 ± 6% for PC3). Cytotoxicity of parent Dox and Dox-loaded GNPs as a function of concentrations is seen in Figure 6c. In addition, the cytotoxicity of the Dox-loaded conjugate toward LNCaP cells was nearly equipotent to that of parent Dox. The observed cytotoxicity of Dox-loaded aptamer-conjugated GNPs is likely attributable to free Dox liberated from the conjugate by diffusion or through degradation of the PSMA aptamer inside cells. Drug release experiments showed that approximately 35% of Dox was released within 1 h, suggesting that drug release was relatively fast (Figure 7).

CONCLUSIONS

In conclusion, by conjugating GNPs with an ONT-hybridized, PSMA-specific aptamer, which forms a GC-rich duplex that acts as a loading site for the chemotherapeutic agent Dox, we have constructed a multifunctional nanoparticle that enables combined prostate cancer imaging by CT and anticancer therapy. PSMA aptamer-conjugated GNPs were able to specifically bind to target prostate cancer cells that overexpressed PSMA antigen, allowing visualization of target-specific binding by silver staining and clinical CT instrumentation. Further, we demonstrated that Dox-loaded aptamer-conjugated GNPs are able to kill target cancer cells more effectively than nontarget cells, suggesting target-specific drug delivery. We anticipate that the present GNP conjugate system could be applied to the design of similar multifunctional NPs through the use of other disease-specific aptamers and imaging nanoprobes.

EXPERIMENTAL SECTION

Measurements: The hydrodynamic particle size of PSMA aptamer-conjugated GNPs was measured using an ELS 8000 light-scattering spectrophotometer (Otsuka Electronics Korea, Seoul, South Korea). Silver-stained cells were visualized using a Leica DMRBE optical microscope (Leica Microsystems AG, Wetzlar, Germany) equipped with 100×, 200×, and 400× objectives. Images were acquired using a CoolSNAPTMfx CCD camera driven by MetaMorph imaging software (Universal Imaging Co, Downingtown, PA). Dox fluorescence was monitored at an excitation wavelength of 480 nm, and emission was recorded over a 500−700 nm interval (3 mm slit) on an RF-5301PC spectrofluorometer (Shimadzu, Kyoto, Japan).

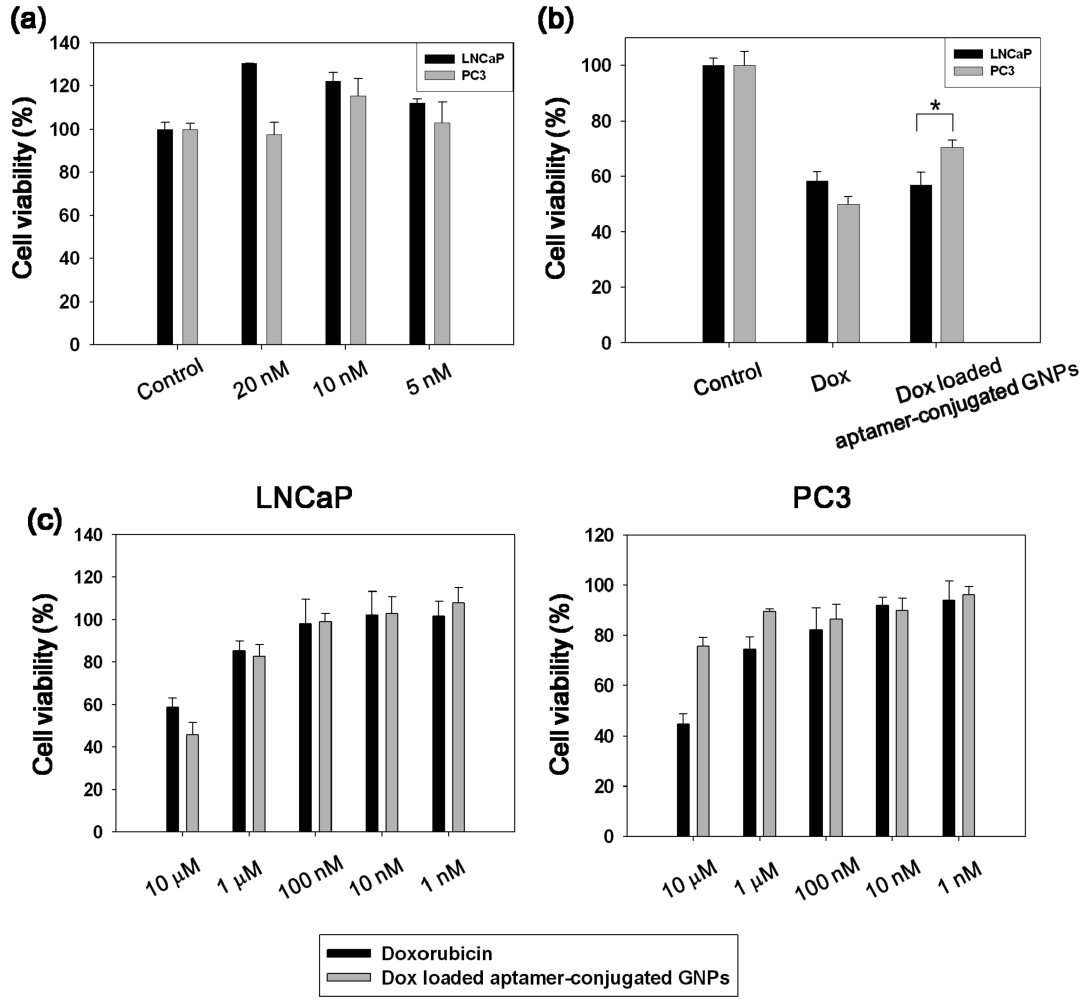

Figure 6. *In vitro* cell viability measured by MTT assays. LNCaP and PC3 cells were incubated with (a) different concentrations of PSMA aptamer-conjugated GNPs for 24 h, (b) free Dox (5 μM) or Dox (5 μM)-loaded PSMA aptamer-conjugated GNPs (8.14 nM), and (c) various concentrations of Dox or Dox-loaded PSMA aptamer-conjugated GNPs for 2 h. Cells were then washed and incubated for an additional 24 h prior to measurement of cell viability as described in the Experimental Section; *$p < 0.05$, LNCaP *versus* PC3 cells ($n = 5$).

Preparation of 13 nm GNPs: In a 250 mL round-bottomed flask equipped with a condenser, 100 mL of 1 mM $HAuCl_4$ was heated to a boil with vigorous stirring. Next, 10 mL of 38.8 mM sodium citrate was added quickly, which resulted in a color change from blue to burgundy. After further stirring at the same temperature for 10 min, the resulting solution was cooled to room temperature.

Aptamer Synthesis: The sequences of the extended PSMA aptamer (A9 CGA aptamer) and the scramble aptamer[20] were 5′-GGG AGG ACG AUG CGG ACC GAA AAA GAC CUG ACU UCU AUA CUA AGU CUA CGU UCC CAG ACG ACU CGC CCG ACG ACG ACG ACG ACG ACG ACG A-3′ and 5′-CAG GCA UGC CUA GCU AAG CAG CCC AUG GCU UAU GCG CGG AAU AUU GGC UUC CGU UCU CGA CGA CGA CGA CGA CGA CGA-3′ (extended sequence of aptamer is underlined), respectively. Each aptamer was synthesized by *in vitro* transcription (12 h at 37 °C) from a double-stranded DNA template that included the T7 RNA promoter using a MEGAscript kit (Ambion, Austin, TX). Following transcription, samples were treated with DNase for 10 min at 37 °C. Aptamers were purified by LiCl precipitation.

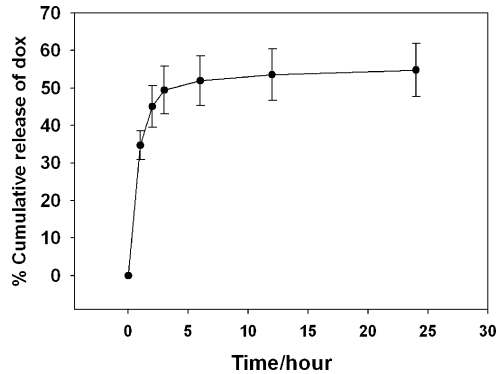

Figure 7. Time-dependent release profile of parent Dox from Dox-loaded PSMA aptamer-conjugated GNPs ($n = 3$).

Conjugation of PSMA Aptamers with GNPs: First, thiol-modified capture ONTs (5′-HS-CC-AAAAAAAAAA-TCGTCGTCGTCGTCGTCG-3′ were added to 13 nm citrated-stabilized GNPs (3 nmol capture ONT per 1 mL of 17 nM GNP). After 16 h, 0.1 M sodium phosphate buffer was added to bring the mixture to 10 mM sodium phosphate, and 1 M sodium chloride was added to bring the sodium chloride concentration to 0.1 M. This solution was gently shaken for an additional 24 h. Next, unreacted capture ONTs were removed by centrifugation at 20 000*g* for 20 min. Then, the extended PSMA aptamer was hybridized to 100 μL of capture ONT-coated GNPs by initially heating the solution at 90 °C for 5 min, followed by incubation at room temperature for 1 h. Unreacted, extended PSMA CGA aptamers were removed by centrifugation at 20 000*g* for 20 min.

Assessment of Cell Binding by Silver Staining: Gelatin-coated coverslips were placed in 24-well plates containing RPMI-1640. LNCaP and PC3 prostate cancer cells were seeded onto each coverslip at a density of 10^5 cells/coverslip and incubated for 24 h. Cells were first preincubated with OPTI-MEM media for 30 min and then incubated with 1 nM PSMA aptamer-conjugated GNPs for 2 h at 37 °C. After incubating with PSMA aptamer-conjugated GNPs, cells were washed three times with PBS, stained using a silver enhancement kit for 5 min, and then washed three more times with PBS. Silver staining results were assessed by light microscopy, as described above.

CT Imaging and HU Measurements: LNCaP and PC3 cell were grown in 100 mm dishes to ~100% confluence. Cells were first preincubated with OPTI-MEM media for 30 min and then incubated with 5 nM PSMA aptamer-conjugated GNPs or 5 nM scramble aptamer-conjugated GNPs for 6 h at 37 °C. Cells were then washed three times with PBS and trypsinized. Approximately 2.5×10^6 cells of each sample were resuspended in 100 μL of PBS. CT data were acquired using a GE Light Speed VCT 64-detector CT (GE Amersham Healthcare System, Milwaukee, WI). Imaging parameters were as follows: slice thickness, 0.625 mm; pitch, 0.984:1; voltage, 80 kVp; current, 500 mA; field of view, 512 × 512, gantry rotation time, 0.4 s; table speed, 40 mm/rotation.

Dox Loading of PSMA Aptamer-Conjugated GNPs: PSMA aptamer-conjugated GNPs (1 nM) were incubated in an aqueous solution of Dox (1 μM) for 1 h. The resulting Dox-loaded PSMA aptamer-conjugated GNPs were collected using a Hanil Supra 22K high-speed centrifuge (Hanil Science Industrial, Incheon, South Korea) at 20 000*g* for 20 min. Then, the amount of unloaded Dox in the supernatant was calculated from the emission intensity of Dox at 550 nm (excitation at 480 nm).

Drug Release Experiment: Dox-loaded aptamer-conjugated GNPs (20 nM GNP) were incubated in PBS with gentle shaking. At the indicated times, PSMA aptamer-conjugated GNPs were collected by centrifugation and the supernatant was removed for fluorescence analysis. The amount of Dox released was determined by fluorescence emission at a λ_{max} of 550 nm, with excitation at 480 nm.

MTT Cell Viability Assay: LNCaP and PC3 cells in RPMI-1640 were grown to 70% confluence in 96-well plates. Before incubation with complex, cells were washed with PBS and incubated with OPTI-MEM media for 30 min. The medium in each well was then replaced with 100 μL of fresh medium containing different concentrations of PSMA aptamer-conjugated GNPs for 24 h or with free Dox (5 μM) or Dox (5 μM)-loaded PSMA aptamer-conjugated GNPs (8.14 nM) for 2 h, washed, and further incubated in fresh media for total of 24 h. After washing the cells twice with PBS, 100 μL of fresh culture medium was added to each well followed by 20 μL of MTT solution (2.5 mg/mL in PBS). The cells were then incubated for an additional 4 h at 37 °C, and then the medium was carefully aspirated. The cells were solubilized in 200 μL of DMSO, and the absorbance in each well at 570 nm was measured using a model FL600 microplate reader (Bio-Tek Inc., Winooski, VT).

Acknowledgment. This work was supported by the Cell Dynamic Research Center, Korean Ministry of Science and Technology (Grant No. R11-2007-007-03002-0) and by a grant from the National R&D Program for Cancer Control, Ministry of Health and Welfare, Republic of Korea (No. 0720210).

Supporting Information Available: ICP-AES, CLSM, and flow cytometry data. This material is available free of charge *via* the Internet at http://pubs.acs.org.

REFERENCES AND NOTES

1. Xu, C.; Xie, J.; Ho, D.; Wang, C.; Kohler, N.; Walsh, E. G.; Morgan, J. R.; Chin, Y. E.; Sun, S. Au-Fe_3O_4 Dumbbell Nanoparticles as Dual-Functional Probes. *Angew. Chem., Int. Ed.* **2008**, *47*, 173–176.
2. Shin, J.; Anisur, R. M.; Ko, M. K.; Im, G. H.; Lee, J. H.; Lee, I. S. Hollow Manganese Oxide Nanoparticles as Multifunctional Agents for Magnetic Resonance Imaging and Drug Delivery. *Angew. Chem., Int. Ed.* **2009**, *48*, 321–324.
3. Kim, J.; Park, S.; Lee, J. E.; Jin, S. M.; Lee, J. H.; Lee, I. S.; Yang, I.; Kim, J.-S.; Kim, S. K.; Cho, M.-H.; Hyeon, T. Designed Fabrication of Multifunctional Magnetic Gold Nanoshells and Their Application to Magnetic Resonance Imaging and Photothermal Therapy. *Angew. Chem., Int. Ed.* **2006**, *45*, 7754–7758.
4. Veiseh, O.; Sun, C.; Gunn, J.; Kohler, N.; Gabikian, P.; Lee, D.; Bhattarai, N.; Ellenbogen, R.; Sze, R.; Hallahan, A.; Olson, J.; Zhang, M. Optical and MRI Multifunctional Nanoprobe for Targeting Gliomas. *Nano Lett.* **2005**, *5*, 1003–1008.
5. Yu, M. K.; Jeong, Y. Y.; Park, J.; Park, S.; Kim, J. W.; Min, J. J.; Kim, K.; Jon, S. Drug-Loaded Superparamagnetic Iron Oxide Nanoparticles for Combined Cancer Imaging and Therapy *In Vivo*. *Angew. Chem., Int. Ed.* **2008**, *47*, 5362–5365.
6. Wang, A. Z.; Bagalkot, V.; Vasilliou, C. C.; Gu, F.; Alexis, F.; Zhang, L.; Shaikh, M.; Yuet, K.; Cima, M. J.; Lnager, R.; Kantoff, P. W.; Bander, N. H.; Jon, S.; Farokhzad, O. C. Superparamagnetic Iron Oxide Nanoparticle−Aptamer Bioconjugates for Combined Prostate Cancer Imaging and Therapy. *ChemMedChem* **2008**, *3*, 1311–1315.
7. Lee, H.; Lee, E.; Kim, D. K.; Jang, N. K.; Jeong, Y. Y.; Jon, S. Antibiofouling Polymer-Coated Superparamagnetic Iron Oxide Nanoparticles as Potential Magnetic Resonance Contrast Agents for *In Vivo* Cancer Imaging. *J. Am. Chem. Soc.* **2006**, *128*, 7383–7389.
8. Lee, H.; Yu, M. K.; Park, S.; Moon, S.; Min, J. J.; Jeong, Y. Y.; Kang, H. W.; Jon, S. Thermally Cross-Linked Superparamagnetic Iron Oxide Nanoparticles: Synthesis and Application as a Dual Imaging Probe for Cancer *In Vivo*. *J. Am. Chem. Soc.* **2007**, *129*, 12739–12745.
9. Gao, X.; Cui, Y.; Levenson, M.; Chung, L. W.; Nie, S. *In Vivo* Cancer Targeting and Imaging with Semiconductor Quantum Dots. *Nat. Biotechnol.* **2004**, *22*, 969–976.
10. Nasongkla, N.; Bey, E.; Ren, J.; Ai, H.; Khemtong, C.; Guthi, J. S.; Chin, S.-F.; Sherry, A. D.; Boothman, D. A.; Gao, J. Multifunctional Polymeric Micelles as Cancer-Targeted, MRI-Ultrasensitive Drug Delivery Systems. *Nano Lett.* **2006**, *6*, 2427–2430.
11. Lee, J.-H.; Lee, K.; Moon, S. H.; Lee, Y.; Park, T. G.; Cheon, J. All-in-One Target-Cell-Specific Magnetic Nanoparticles for Simultaneous Molecular Imaging and siRNA Delivery. *Angew. Chem., Int. Ed.* **2009**, *48*, 4174–4179.
12. Kohler, N.; Sun, C.; Fichtenholtz, A.; Gunn, J.; Fang, C.; Zhang, M. Methotrexate-Immobilized Poly(ethylene glycol) Magnetic Nanoparticles for MR Imaging and Drug Delivery. *Small* **2006**, *2*, 785–792.
13. Bagalkot, V.; Zhang, L.; Levy-Nissenbaum, E.; Jon, S.; Kantoff, P. W.; Farokhzad, O. C. Quantum Dot−Aptamer Conjugates for Synchronous Cancer Imaging, Therapy, and Sensing of Drug Delivery Based on Bi-Fluorescence Resonance Energy Transfer. *Nano Lett.* **2007**, *7*, 3065–3070.
14. Derfus, A. M.; Chen, A. A.; Min, D.-H.; Ruoslahti, E.; Bhatia, S. N. Targeted Quantum Dot Conjugates for siRNA Delivery. *Bioconjugate Chem.* **2007**, *18*, 1391–1396.
15. Walther, C.; Meyer, K.; Rennert, R.; Neundorf, I. Quantum Dot−Carrier Peptide Conjugates Suitable for Imaging and Delivery Applications. *Bioconjugate Chem.* **2008**, *19*, 2346–2356.
16. Loo, C.; Lowery, A.; Halas, N.; West, J.; Drezek, R. Immunotargeted Nanoshells for Integrated Cancer Imaging and Therapy. *Nano Lett.* **2005**, *5*, 709–711.
17. Huang, X.; El-Sayed, I. H.; Qian, W.; El-Sayed, M. A. Cancer Cell Imaging and Photothermal Therapy in the Near-Infrared Region by Using Gold Nanorods. *J. Am. Chem. Soc.* **2006**, *128*, 2115–2120.
18. Kim, D.; Park, S.; Lee, J. H.; Jeong, Y. Y.; Jon, S. Antibiofouling Polymer-Coated Gold Nanoparticles as a Contrast Agent for *In Vivo* X-ray Computed Tomography Imaging. *J. Am. Chem. Soc.* **2007**, *129*, 7661–7665.
19. Popovtzer, R.; Agrawal, A.; Kotov, N. A.; Popovtzer, A.; Balter, J.; Carey, T. E.; Kopelman, R. Targeted Gold Nanoparticles Enable Molecular CT Imaging of Cancer. *Nano Lett.* **2008**, *8*, 4593–4596.

20. Lupold, S. E.; Hicke, B. J.; Lin, Y.; Coffey, D. S. Identification and Characterization of Nuclease-Stabilized RNA Molecules That Bind Human Prostate Cancer Cells *via* the Prostate-Specific Membrane Antigen. *Cancer Res.* **2002**, *62*, 4029–4033.
21. Farokhzad, O. C.; Jon, S.; Khademhosseini, A.; Tran, T.-N. T.; LaVan, D. A.; Langer, R. Nanoparticle−Aptamer Bioconjugates. *Cancer Res.* **2004**, *64*, 7668–7672.
22. Farokhzad, O. C.; Cheng, J.; Teply, B. A.; Sherifi, I.; Jon, S.; Kantoff, P. W.; Richie, J. P.; Langer, R. Targeted Nanoparticle−Aptamer Bioconjugates for Cancer Chemotherapy *In Vivo*. *Proc. Natl. Acad. Sci. U.S.A.* **2006**, *103*, 6315–6320.
23. Cao, Z.; Tong, R.; Mishra, A.; Xu, W.; Wong, G. C. L.; Cheng, J.; Lu, Y. Reversible Cell-Specific Drug Delivery with Aptamer-Functionalized Liposomes. *Angew. Chem., Int. Ed.* **2009**, *48*, 6494–6498.
24. Dassiel, J. P.; Liu, X.; Thomas, G. S.; Whitaker, R. M.; Thiel, K. W.; Stockdale, K. R.; Meyerholz, D. K.; McCaffrey, A. P.; McNamara, J. O.; Giangrande, P. H. Systemic Administration of Optimized Aptamer−siRNA Chimeras Promotes Regression of PSMA-Expressing Tumors. *Nat. Biotechnol.* **2009**, *27*, 839–846.
25. Ng, E. W. M.; Shima, D. T.; Calias, P.; Cunningham Jr, E. T.; Guyer, D. R.; Adamis, A. P. Pegaptanib, a Targeted Anti-VEGF Aptamer for Ocular Vascular Disease. *Nat. Rev. Drug Discovery* **2006**, *5*, 123–132.
26. Bagalkot, V.; Farokhzad, O. C.; Langer, R.; Jon, S. An Aptamer-Doxorubicin Physical Conjugate as a Novel Targeted Drug-Delivery Platform. *Angew. Chem., Int. Ed.* **2006**, *45*, 8149–8152.
27. Chaires, J. B.; Herrera, J. E.; Waring, M. J. Preferential Binding of Daunomycin to 5′TACG and 5′TAGC Sequences Revealed by Footprinting Titration Experiments. *Biochemistry* **1990**, *29*, 6145–6153.
28. Liu, J.; Lu, Y. Preparation of Aptamer-Linked Gold Nanoparticle Purple Aggregates for Colorimetric Sensing of Analytes. *Nat. Protoc.* **2006**, *1*, 246–252.
29. Javier, D. J.; Nitin, N.; Levy, M.; Ellington, A.; Richards-Kortum, R. Aptamer-Targeted Gold Nanoparticles as Molecular-Specific Contrast Agents for Reflectance Imaging. *Bioconjugate Chem.* **2008**, *19*, 1309–1312.
30. Jin, R.; Wu, G.; Li, Z.; Mirkin, C. A.; Schatz, G. C. What Controls the Melting Properties of DNA-Linked Gold Nanoparticle Assemblies? *J. Am. Chem. Soc.* **2003**, *125*, 1643–1654.